Microstructural controls on thermal cracking in igneous rocks

John Browning[1*], Philip G. Meredith[2^], Ali Daoud[2] and Thomas Mitchell[2]

[1] Department of Mining Engineering and Department of Structural and Geotechnical Engineering, Pontificia Universidad Católica de Chile, Santiago, Chile

[2] Department of Earth Sciences, University College London, London, UK

* Corresponding author information: jbrowning@ing.puc.cl

^ Presenting author

1. Introduction

Crack damage induced in rocks by thermal stresses is an important process in both geology and geomorphology. Geologically, it reduces rock strength and contributes to enhanced fluid storage and flow, while, geomorphologically, it can provide a crucial contribution to mechanical weathering and, hence, landform evolution. Crack damage due to thermal stresses can be induced in rocks during heating, under all-round compression; during cooling, under all-round tension; and is commonly also enhanced by temperature cycling. Whilst there remains a paucity of data relating to cyclic thermal stressing in rocks, previous studies have demonstrated that, for some rocks the great majority of thermal cracking is generated during heating, while for other rocks most of the cracking is generated during cooling. Here, we report results from thermal stressing experiments on three rocks with different mineralogical compositions and microstructures in which we use acoustic emission (AE) output as a measure of the timing and amount of thermal cracking.

2. Methods and materials

Core samples, measuring 25 mm in diameter by 65 mm in length, were held within a purpose-built heating jig manufactured from 310 stainless steel alloy, capable of sustaining temperatures up to 1100°C without significant corrosion. The jig is approximately 1 m in length and comprises a series of rods and springs to hold the sample under constant end-load within the central, uniform temperature section, of a Carbolite CTF12/75/700 tube furnace while allowing for expansion and contraction (Figure 1) (see also; Browning et al., 2016; Castagna et al., 2018; Daoud et al., 2020). The central rods act as acoustic waveguides and are of sufficient length to enable an AE transducer to be located outside of the furnace where it remains cool. The external springs allow the central rods to move in response to sample expansion and contraction during heating and cooling and therefore maintain a uniform contact throughout the experiments. Temperature was monitored by a thermocouple placed on the sample surface and controlled using a calibrated thermocouple contained within the tube furnace. All experiments were conducted at ambient pressure.

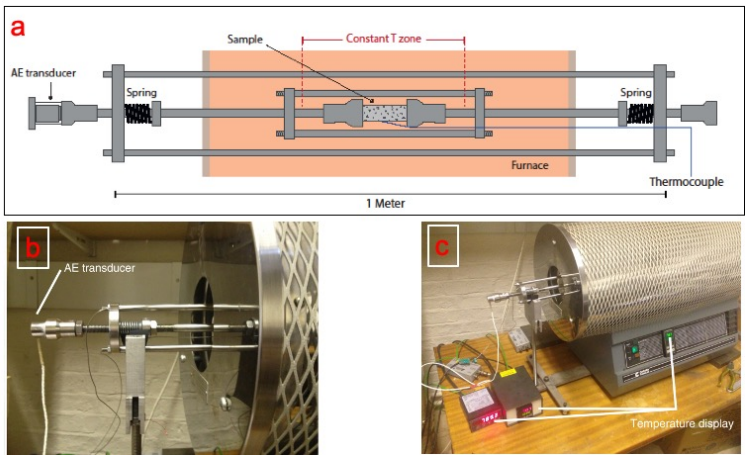

Figure 1. Schematic diagram and images of the experimental arrangement used for the cyclic thermal stressing experiments

Three intrusive igneous rocks were selected for our thermal stressing tests (Figure 2). A coarse-grained granophyre from the Slaufrudalur pluton in Eastern Iceland (SGP) (Burchardt et al., 2012; Browning et al., 2016), a bi-modal grain-sized andesite from Santorini (SA), and a finer grained basalt from the Seljadalur region of SW Iceland (SB). SGP is an intrusive granophyre from a pluton, with an initial porosity of around 2% (Browning et al,, 2016) and a microstructure dominated by

> 1 mm interlocked quartz grains. SA is an intrusive andesite, with a relatively high initial porosity of around 13%, comprised of primarily open vesicular pores with some pre-existing microcracks that primarily emanate from vesicle boundaries. The microstructure of SA comprises large (>0.5 mm) plagioclase crystals embedded within a much finer-grained matrix. SB is an intrusive, tholeitic basalt, with an initial porosity of around 4% (Vinciguerra et al., 2005; Browning et al., 2016). Its microstructure is dominated by an intergranular matrix of plagioclase, pyroxene and iron oxides.

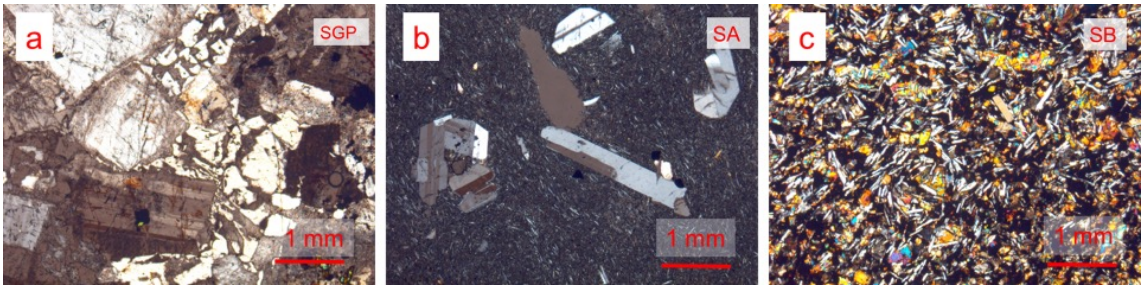

Figure 2. The three materials studied a) Granophyre from Eastern Iceland (SGP), b) Andesite from Santorini, Greece (SA), c) Basalt from Seljadalur Iceland (SB). SGP is dominated by > 1mm interlocked quartz grains, whereas SA has a very fine-grained Plg/Px matrix with larger (>0.5 mm) plagioclase crystals embedded. SB consists of plagioclase laths within a finer-grained matrix of Ol/Px crystals.

3. Results

We present results from two suites of thermal stressing tests. In the first suite (Figure 3), samples of each rock type were individually subjected to a single heating and cooling cycle to a maximum temperature of 900°C. In these tests, the samples were heated at a rate of 1°C/min, held at the maximum temperature for 30 minutes and then cooled at a natural cooling rate that did not exceed 1°C/min. In the second suite (Figure 4), samples were subjected to multiple heating and cooling cycles to peak temperatures of 350°C, 500°C, 700°C and 900°C (all at a constant rate of 1°C/min on heating and a natural cooling rate of <1°C/min)..

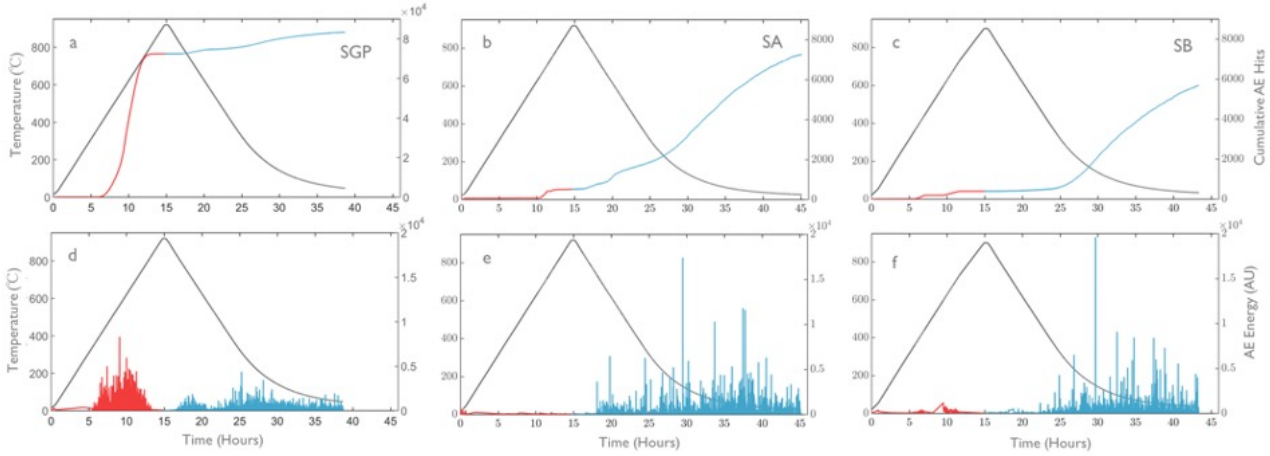

Figure 3. Cumulative acoustic emission hits generated during heating (in red) and cooling (in blue) from 900°C in the three rock types, a) Slaufrudalar Granophyre (SGP), b) Santorini Andesite (SA), and c) Seljadalur Basalt (SB) with Acoustic Emission hit energy recorded in d, e, and f. NOTE: Order of magnitude difference in AE totals between SGP (a,d) and SA/SB (b,c,e,f).

In the single heating and cooling cycle test on SGP, both the cumulative number of AE hits and the AE energy output are notably higher during the heating phase than during the cooling phase (Fig. 3, a, d). In total, some 83,000 AE hits were recorded, and over 72,000 (87%) of these were generated during the heating phase. By contrast, the output of AE for the same type of test, for both SA and SB is much greater during the cooling phases than during the heating phases (Fig. 3, b, c, e, f). For SA, a total of just over 7000 AE hits are generated during the whole test, with over 90% being generated during the cooling phase. Similarly, well over 90% of the AE energy is generated during this phase. A similar pattern is observed for SB, with over 90% of the 6000 recorded AE hits and over 90% of the AE energy being generated during the cooling phase.

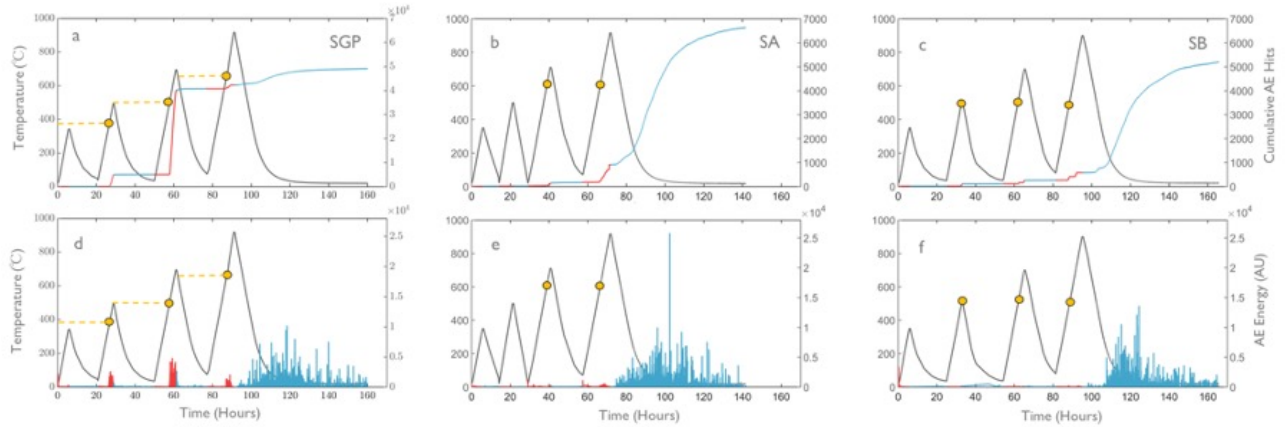

Figure 4. Cumulative AE hits (a, b, c) and AE energy (d, e, f) generated during multiple cyclic heating (in red) and cooling (in blue) to peak temperatures of 350 °C, 500 °C, 700 °C and 900 °C in SGP, SA, and SB, respectively. Orange dots indicate the onset of AE output in each cycle where significant AE was generated. Note the order of magnitude difference in the scale of cumulative AE hits between SGP (a) and SA/SB (b,c).

In the thermal cycling test on SGP (Figure 4 a, d) we observe essentially no AE output during either the heating or cooling phases of the first cycle to a temperature peak of 350°C. By contrast, during the second heating cycle we observe the onset of significant AE output around 380°C, which continues at a relatively constant rate until the temperature peak of 500°C is reached. We then observe essentially zero AE output during the cooling phase of this cycle (Fig. 4, a, d). We also note that during the third heating cycle the AE output re-commenced at 500°C, significantly higher than the onset temperature of 380°C in the previous cycle. Significantly, this corresponds both to the maximum temperature in the previous cycle and the point at which AE output ceased during that cycle. This observation suggests the presence of 'temperature-memory' effect, analogous to the Kaiser stress memory effect reported in numerous studies of cyclic mechanical loading of rocks (Lockner, 1993; Holcomb, 1993; Lavrov, 2001; Lavrov, 2003; Browning et al., 2018). The AE output continued to increase steadily until the temperature peak of 700°C was reached. A relatively small amount of AE output occurred during the very earliest part of the cooling phase, but ceased after that, with essentially nothing being recorded during the remainder of the cooling phase. A similar pattern of activity was observed during the final cycle, with the heating being essentially aseismic until a temperature of 680°C was reached. This is close to the previous maximum temperature and also corresponds to the temperature at which AE ceased during the cooling phase of the previous cycle. This observation therefore adds further support to the idea of a temperature-memory effect in SGP.

The results from the thermal cycling tests on both SA (Figure 4b, e) and SB (Figure 4c, f) were very similar to each other, but quite different from those for SGP, although all three rocks were exposed to identical thermal cycling to the same set of peak temperatures. During the thermal cycling test on SA we recorded no significant AE during the first two cycles of heating and cooling to peak temperatures of 350°C and 500°C. The first onset of AE output occurs around 600°C during the heating phase of the third cycle, but both the number of hits and the energy are rather low. Significantly more AE is generated during the phase of cooling from the temperature peak of 700°C. During the final cycle, we again observe an AE onset at the same temperature of 600°C during the heating phase, and the output continues up to the maximum temperature of 900°C.

4. Conclusions

Our experimental results demonstrate clearly that the acoustic emission (AE) behavior of SGP during thermal stressing is fundamentally different from that of both SA and SB, whereas the patterns of behavior of SA and SB are essentially the same. SGP is a tightly-packed, coarse-grained rock with a microstructure dominated by interlocking quartz grains. It is well-known that the thermal expansion coefficients of quartz are highly anisotropic, with the *a*-axis value being around 2 times the *c*-axis value (Meredith et al., 2001). It has been concluded that the mechanism responsible for thermal cracking in quartz-rich rocks is most likely to be splitting of individual grains due to the compressive stress generated along their *a*-axes, aided by the small tensile stress generated along their *c*-axes, during heating (Meredith et al., 2001). Conversely, the low level of cracking that occurs during cooling of SGP is likely associated with grain realignment and sliding and some

extension of pre-existing thermal cracks during contraction, as suggested by Griffiths et al. (2018). By contrast, the microstructure of SA comprises large angular plagioclase crystals embedded within a much finer-grained matrix, while SB comprises smaller, partially-oriented plagioclase crystals in a finer-grained matrix with an interstitial glass phase. We simplify this for both SA and SB by considering the phenocrysts as acting as elastic inclusions within an essentially homogeneous matrix using the model of Fredrich and Wong (1981) and Browning et al., (2016). This allows us to conclude that the sparse and low energy AE events generated in SA and SB during heating are likely due to small increments of extension of pre-existing grain boundary cracks and the growth of relatively small numbers of new, intragranular cracks, within an overall compressional regime. By contrast, the numerous and higher energy AE events generated during cooling are likely due to the growth of large numbers of full-length grain boundary cracks together with a significant number of intragranular cracks of more limited extent, within an overall tensile regime. Since our interpretation is that very few, and only partial, cracks are induced during heating in SA and SB, large numbers of potential crack nucleation and extension sites remain. It is therefore not surprising that cracking can recommence at these sites at the same onset temperature (and same thermally-induced stress) in subsequent heating phases during multiple thermal cycling tests (Figure 4b, c).

Appreciation of both the micromechanics operating in rocks of different compositions and the cyclicity of temperature changes is necessary to correctly understand the role of thermal cracking in surface deposits.

5. Acknowledgements

This work was partly funded by NERC award NE/N002938/1, which we gratefully acknowledge. JB also acknowledges support from Fondecyt award 11190143 and Fondap-Conicyt 15090013. We are grateful for continuous support from S. Boon and N. Hughes who were heavily involved with the experimental apparatus design.

6. References

Burchardt, S., Tanner, D., Krumbholz, M., 2012. The Slaufrudalur pluton, southeast Iceland—an example of shallow magma emplacement by coupled cauldron subsidence and magmatic stoping. *Bulletin*, *124*(1-2), pp.213-227.

Browning, J., Meredith, P.G., Gudmundsson, A. 2016. Cooling-dominated cracking in thermally stressed volcanic rocks, *Geophys. Res. Lett.,* **43**, doi:10.1002/2016GL070532

Browning, J., Meredith, P.G., Stuart, C., Harland, S., Healy, D. and Mitchell, T.M., 2018. A directional crack damage memory effect in sandstone under true triaxial loading. Geophysical Research Letters, 45(14), pp.6878-6886.

Castagna, A., Ougier-Simonin, A., Benson, P.M., Browning, J., Walker, R.J., Fazio, M. and Vinciguerra, S., 2018. Thermal Damage and Pore Pressure Effects of the Brittle-Ductile Transition in Comiso Limestone. *Journal of Geophysical Research: Solid Earth*, *123*(9), pp.7644-7660.

Daoud, A., Browning, J., Meredith, P.G., Mitchell, T. 2020. Microstructural controls on thermal crack damage and the presence of a temperature-memory effect during cyclic thermal stressing of rocks. Geophysical Research Letters. 47.

Fredrich, J. T., and Wong, T. 1986. Micromechanics of thermally induced cracking in three crustal rocks. *J. Geophys. Res.*, **91**. 12743-12764

Griffiths, L., Lengliné, O., Heap, M.J., Baud, P. and Schmittbuhl, J., 2018. Thermal cracking in Westerly Granite monitored using direct wave velocity, coda wave interferometry, and acoustic emissions. Journal of Geophysical Research: Solid Earth, 123(3), pp.2246-2261.

Holcomb, D.J., 1993. General theory of the Kaiser effect. International Journal of Rock Mechanics and Mining Sciences & Geomechanics Abstracts, . 30, 7, 929-935

Lavrov, A., 2001. Kaiser effect observation in brittle rock cyclically loaded with different loading rates. Mechanics of Materials, 33(11), pp.669–677.

Lockner, D., 1993. The role of acoustic emission in the study of rock fracture. International Journal of Rock Mechanics and Mining Sciences & Geomechanics Abstracts, 30(7), pp.883-899.

Vinciguerra, S., Trovato, C., Meredith, P.G. and Benson, P.M. 2005, Relating seismic velocities, thermal cracking and permeability in Mt. Etna and Iceland basalts, *Int. J. Rock Mech. Min. Sci.,* **42**, 900–910.